Bending response of functionally graded piezoelectric plates using a two-variable shear deformation theory

Ashraf M. Zenkour[*1,2] and Zahra S. Hafed[1,3]

[1]Department of Mathematics, Faculty of Science, King Abdulaziz University, Jeddah 21589, Saudi Arabia
[2]Department of Mathematics, Faculty of Science, Kafrelsheikh University, Kafrelsheikh 33516, Egypt
[3]Department of Mathematics, Faculty of Science, King Khaled University, Abha 21589, Saudi Arabia

Abstract.   This paper proposes a bending analysis for a functionally graded piezoelectric (FGP) plate through utilizing a two-variable shear deformation plate theory under simply-supported edge conditions. The number of unknown functions used in this theory is only four. The electric potential distribution is assumed to be a combination of a cosine function along the cartesian coordinate. Applying the analytical solutions of FGP plate by using Navier's approach and the principle of virtual work, the equilibrium equations are derived. The paper also discusses thoroughly the impact of applied electric voltage, plate's aspect ratio, thickness ratio and inhomogeneity parameter. Results are compared with the analytical solution obtained by classical plate theory, first-order-shear deformation theory, higher-order shear deformation plate theories and quasi-three-dimensional sinusoidal shear deformation plate theory.

Keywords: FG plate; piezoelectric; bending; two-variable shear plate theory; Navier's method

1. Introduction

The functionally graded materials (FGMs) are defined as a class of composites which possess constant variation of the properties of material from a given surface to another eradicating the stress concentration in laminated composites. Typically, FGMs are consist of a blend of metal and ceramic. Although such materials are usually isotropic, they are nonhomogeneous. The reason why FGMs are especially interesting is because some types of FGM structures can be created which can be able to adapt to various conditions of operation. The rising rates of the applications of FGM make it necessary to have accurate models with responses that can be accurately predicted.

Using a Fourier-based approach, Chi and Chung (2006) employed the classical plate theory (CPT) to obtain an elastic analysis for an FG plate which was applied to transverse loads. Jha *et al*. (2013) provided a critical review of more recent studies on the static stability analysis and vibration of FG rectangular plates. The usual refined theory considered in the treatment of the dynamic bending response of flat orthotropic plates is the simple first-order shear deformation theory (FSDT). The theory was designed for statics by Reissner (1944), (1945) yet extended to dynamics by Mindlin (1951). The in-plane displacements in this theory are prolonged to the first

---

term in the thickness coordinate. However, the rotations of normal to the mid-surface are considered independent of the transverse deflection. Any vibrational principle for FSDT can be employed to derive a reliable set of differential equations that govern the plate motion. Because the shear deformation has substantial impacts on the FG rectangular plates responses, shear deformation theories (e.g., FSDT and higher-order shear deformation plate theories (HSDTs)) should be used in the FG rectangular plate analysis. The FSDT accounts for the transverse shear deformation effects by linear variation for the in-plane displacements through the thickness of the plate and needs a shear correction factor while the HSDTs account for the transverse shear deformation effects by higher-order theory variations for in-plane displacements or both in-plane and transverse displacements. For instance, a third-order shear deformation plate theory (TSDT) was developed by Reddy (1984), (2000) with cubic variations for in-plane displacements. Moreover, based on Carrera's unified formulation, Neves *et al*. (2013) managed to develop an HSDT with cubic and parabolic variations of the in-plane and transverse displacements, in respective order. Matsunaga (2009) used an HSDT for the 2D nonlinear analysis of an FG rectangular plate subjected to mechanical and thermal loads. Also, Ghasemabadian and Kadkhodayan (2016) used the HSDT to investigate the buckling FGP plates using circuit conditions.

Along with the utilize of polynomial functions in above-mentioned works, trigonometric functions are used for the purpose of developing HSDTs. For example, Zenkour (2006) proposed a generalized shear deformation plate theory for FG in which the in-plane deflections are expanded as sinusoidal species through the thickness (see also, Zenkour (2004, 2005a, b, c, 2007, 2009)). Mantari *et al*. (2012a, b, c) and Mantari and Guedes Soares (2012) presented trigonometric shear deformation plate theories which represent optimal distribution of through-the-thickness transverse strains and meet the free stress boundary conditions on the surface of the plate without employing a shear correction factor. Relying on Carrera's unified formulation, Ferreira *et al*. (2011) expanded an HSDT with the uses of sinusoidal functions in terms of thickness for both in-plane and transverse displacement components, whereas Neves *et al*. (2012a, b) presented HSDTs with the use of various expansions i.e., sinusoidal (Neves *et al*. 2012a) or hyperbolic shear deformation plate theory (Neves *et al*. 2012b).

Some of the HSDTs mentioned above are computational costs because of additional unknown variables that are introduced to the theory such as the theories proposed by Pradyumna and Bandyopadhyay (2008) and Neves *et al*. (2012a), (2013) with nine unknown variables, Reddy (2011) with eleven unknown variables; Tu *et al.* (2017) with eight unknown variables; and Talha and Singh (2010) with thirteen unknown variables. Even though some popular HSDTs have five unknowns such as the TSDT of Reddy (2000), the quasi-3D HSDT of Benbakhti *et al.* (2016), the sinusoidal and trigonometric shear plates deformation theories of Mantari *et al*. (2012a, b, c) and Zenkour and Aljadani (2018). The motion equations of such theories are far more sophisticated than those pertinent to the FSDT. Therefore, they require the developing a shear deformation theory that can be handy to use.

Jandaghian and Rahmani (2017) discussed the problem of thermo-electro-mechanical vibration of the FGP nanoplates subjected to applied biaxial forces and electric voltage with uniform temperature. Arefi and Zenkour (2016a, b; 2017a, b, c) concluded some valuable findings pertinent to the electro-elastic analysis of FG plates structures. More elaboration can be obtained from the studies Giannakopoulos and Suresh (1999), Liew *et al*. (2004), Gürses *et al*. (2009), Baltacioglu *et al*. (2010), Fereidoon *et al*. (2011) and Demir *et al*. (2016). The free vibration analyses of smart annular FG rectangular plate integrated with two uniformly piezoelectric layers put at the bottom

and the top of the structure was carried out by Ebrahimi and Rastgoo (2008) by using the CPT.

In this study, a simple two-variable shear deformation plate theory is analyzed for the bending analyses of FGP plates. Although the current theory has only five unknowns (four mechanical displacements and one electric potential) and five governing equations, it successfully meets the boundary requirements on the top and bottom surfaces of the plate without any shear correction factors. The mechanical response of FG plates with piezoelectric effect is presented via applying the present theory. The plate is also subjected to mechanical electrical loads. The effect of gradient index, side-to-thickness ratio, plate aspect ratio and electric loading on the electric displacement, electric potential, displacement and stress are presented. The influences of applied electric voltage and other parameters are also discussed in this study.

2. Formulation of the problem

The FGP plate is shown in Fig. 1. The length of the plate is a, width is b and uniform thickness is h. An orthogonal coordinate axes, x, y and z is then selected. The effective properties P of the FGP material, namely, Young's modulus E and Poisson's ratio v are continuously varied in the thickness direction according to the following formula:

$$P(z) = P_m + (P_c - P_m)\left(\frac{1}{2} + \frac{z}{h}\right)^k, \qquad k \geq 0, \tag{1}$$

where P_m and P_c represent the properties of the metal and ceramic, respectively, and k denotes the non-negative gradient index. The plate is pure ceramic when k equals to zero and and if k approaches infinity then a pure metallic plate in the case.

The displacement components of the FGP plate are assumed with the aid of the simple two-variable HSDT are expressed as (Bouazza *et al.* 2018, Zenkour 2013a, b, c, 2015)

$$u(x,y,z) = u(x,y) - z\frac{\partial w_b}{\partial x} - f(z)\frac{\partial w_s}{\partial x},$$
$$v(x,y,z) = v(x,y) - z\frac{\partial w_b}{\partial y} - f(z)\frac{\partial w_s}{\partial y}, \tag{2}$$
$$w(x,y,z) = w_b(x,y) + w_s(x,y),$$

where $f(z) = z - \frac{4z^3}{3h^2}$. Also, u, v and w denote the displacements in the directions of x, y and z, respectively; w_s, w_b denote shear and bending components of the vertical displacement w.

By using Eq. (2), the strain field can be expressed as

$$\varepsilon_x = \frac{\partial u}{\partial x} - z\frac{\partial^2 w_b}{\partial x^2} - f(z)\frac{\partial^2 w_s}{\partial x^2},$$
$$\varepsilon_y = \frac{\partial v}{\partial y} - z\frac{\partial^2 w_b}{\partial y^2} - f(z)\frac{\partial^2 w_s}{\partial y^2},$$
$$\gamma_{xy} = \frac{\partial u}{\partial y} + \frac{\partial v}{\partial x} - 2z\frac{\partial^2 w_b}{\partial x\partial y} - 2f(z)\frac{\partial^2 w_s}{\partial x\partial y}, \tag{3}$$
$$\gamma_{yz} = g(z)\frac{\partial w_s}{\partial y}, \qquad \gamma_{xz} = g(z)\frac{\partial w_s}{\partial x},$$
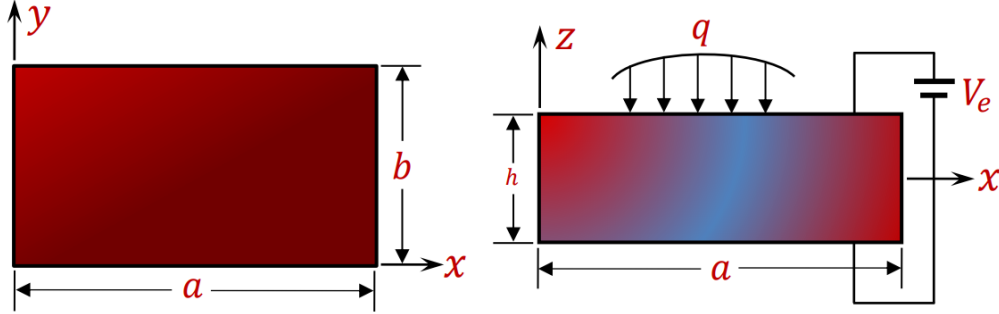
Fig. 1 Coordinates and formulation of the FGP plate

where $g(z) = 1 - \frac{4z^2}{h^2}$. The stress-strain relations for the FGP plate are expressed as:

$$\begin{Bmatrix} \sigma_x \\ \sigma_y \\ \tau_{yz} \\ \tau_{xz} \\ \tau_{xy} \end{Bmatrix} = \begin{bmatrix} c_{11} & c_{12} & 0 & 0 & 0 \\ c_{12} & c_{22} & 0 & 0 & 0 \\ 0 & 0 & c_{44} & 0 & 0 \\ 0 & 0 & 0 & c_{55} & 0 \\ 0 & 0 & 0 & 0 & c_{66} \end{bmatrix} \begin{Bmatrix} \varepsilon_x \\ \varepsilon_y \\ \gamma_{yz} \\ \gamma_{xz} \\ \gamma_{xy} \end{Bmatrix} - \begin{bmatrix} 0 & 0 & e_{31} \\ 0 & 0 & e_{32} \\ 0 & e_{24} & 0 \\ e_{15} & 0 & 0 \\ 0 & 0 & 0 \end{bmatrix} \begin{Bmatrix} E_x \\ E_y \\ E_z \end{Bmatrix}, \tag{4a}$$

$$\begin{Bmatrix} D_x \\ D_y \\ D_z \end{Bmatrix} = \begin{bmatrix} 0 & 0 & 0 & e_{15} & 0 \\ 0 & 0 & e_{24} & 0 & 0 \\ e_{31} & e_{32} & 0 & 0 & 0 \end{bmatrix} \begin{Bmatrix} \varepsilon_x \\ \varepsilon_y \\ \gamma_{yz} \\ \gamma_{xz} \\ \gamma_{xy} \end{Bmatrix} + \begin{bmatrix} \mu_{11} & 0 & 0 \\ 0 & \mu_{22} & 0 \\ 0 & 0 & \mu_{33} \end{bmatrix} \begin{Bmatrix} E_x \\ E_y \\ E_z \end{Bmatrix}, \tag{4b}$$

where σ_{ij}, ε_{ij}, D_i and E_i represent the stress tensor, strain tensor, electric displacement vector and electric field, respectively; e_{ij} and μ_{ik} denote piezoelectric and permittivity coefficients respectively. The elastic coefficients c_{ij} for the FGP plate are:

$$c_{11} = c_{22} = \frac{E}{1 - v^2}, \quad c_{12} = \frac{vE}{1 - v^2}, \quad c_{ii} = \frac{E}{2(1 + v)}, \quad (i = 4,5,6). \tag{5}$$

The non-zero components of electric field with the electric potential are defined as:

$$\begin{Bmatrix} E_x \\ E_y \\ E_z \end{Bmatrix} = - \begin{Bmatrix} \frac{\partial \phi}{\partial x} \\ \frac{\partial \phi}{\partial y} \\ \frac{\partial \phi}{\partial z} \end{Bmatrix}. \tag{6}$$

To get the components of electric field tensor, the distribution of the electric potential must be determined. In the current analysis, electrical potential is supposed to be a combination of cosine and linear variation as following form

$$\phi(x, y, z) = \frac{2z}{h} \psi_0 - \cos(\xi z) \, \psi(x, y), \tag{7}$$

where $\psi(x, y)$ represents the electric potential on the mid-plane, $\xi = \frac{\pi}{h}$ and ψ_0 denotes the external electric voltage applied to upper and lower surfaces of the FGP plate.

From Eq. (7), the components of electric field can be written as:

$$\begin{Bmatrix} E_x \\ E_y \\ E_z \end{Bmatrix} = \begin{Bmatrix} \dfrac{\partial \psi}{\partial x} \cos(\xi z) \\[2mm] \dfrac{\partial \psi}{\partial y} \cos(\xi z) \\[2mm] -\dfrac{2\psi_0}{h} - \xi \sin(\xi z)\psi \end{Bmatrix}. \tag{8}$$

The principle of virtual work is proposed to obtain the equilibrium equations in the form

$$\int_{\Omega} \int_{-h/2}^{h/2} (\sigma_x \delta\varepsilon_x + \sigma_y \delta\varepsilon_y + \tau_{yz}\delta\gamma_{yz} + \tau_{xz}\delta\gamma_{xz} + \tau_{xy}\delta\gamma_{xy}) \, \mathrm{d}z \, \mathrm{d}\Omega$$

$$-\int_{\Omega} \int_{-\frac{h}{2}}^{\frac{h}{2}} (D_x \delta E_x + D_y \delta E_y + D_z \delta E_z) \mathrm{d}z \, \mathrm{d}\Omega - \int_{\Omega} q(\delta w_b + \delta w_s)\mathrm{d}\Omega = 0, \tag{9}$$

where h denotes the total thickness of the plate. By using the Eqs. (3), (4) and (8) into Eq. (9) and integrating through the plate thickness, one can obtain

$$\iint_{\Omega} \left\{ N_x \frac{\partial \delta u}{\partial x} - M_x \frac{\partial^2 \delta w_b}{\partial x^2} - P_x \frac{\partial^2 \delta w_s}{\partial x^2} + N_y \frac{\partial \delta v}{\partial y} - M_y \frac{\partial^2 \delta w_b}{\partial y^2} - P_y \frac{\partial^2 \delta w_s}{\partial y^2} \right.$$

$$+ N_{xy} \left(\frac{\partial \delta u}{\partial y} + \frac{\partial \delta v}{\partial x} \right) - 2M_{xy} \frac{\partial^2 \delta w_b}{\partial x \partial y} - 2P_{xy} \frac{\partial^2 \delta w_s}{\partial x \partial y} + Q_{yz} \frac{\partial \delta w_s}{\partial y} + Q_{xz} \frac{\partial \delta w_s}{\partial x} \tag{10}$$

$$\left. - \widehat{D}_x \frac{\partial \delta \psi}{\partial x} - \widehat{D}_y \frac{\partial \delta \psi}{\partial y} + \widehat{D}_z \delta\psi - q(\delta w_b + \delta w_s) \right\} \mathrm{d}\Omega = 0,$$

where (N_x, N_y, N_{xy}) are called the in-plane force resultant, (M_x, M_y, M_{xy}) are called the moment resultants, (Q_x, Q_y) are called the transverse force resultants and piezoelectric forces $(\widehat{D}_x, \widehat{D}_y, \widehat{D}_z)$ defined as

$$\{N_i, M_i, P_i\} = \int_{-h/2}^{h/2} \sigma_i \{1, z, f(z)\}\mathrm{d}z, \qquad i = x, y,$$

$$\{N_{xy}, M_{xy}, P_{xy}\} = \int_{-h/2}^{h/2} \sigma_{xy}\{1, z, f(z)\}\mathrm{d}z,$$

$$Q_{iz} = \int_{-h/2}^{h/2} g(z)\sigma_{iz}\mathrm{d}z, \qquad i = x, y, \tag{11}$$

$$\{\widehat{D}_i, \widehat{D}_z\} = \int_{-h/2}^{h/2} \{D_i \cos(\xi z), D_z \xi \sin(\xi z)\}\mathrm{d}z, \qquad i = x, y.$$

The expressions of stress and moments resultants can be written as:

$$N_x = A_{11}\frac{\partial u}{\partial x} + A_{12}\frac{\partial v}{\partial y} - B_{11}\frac{\partial^2 w_b}{\partial x^2} - B_{12}\frac{\partial^2 w_b}{\partial y^2} - B_{11}^a\frac{\partial^2 w_s}{\partial x^2} - B_{12}^a\frac{\partial^2 w_s}{\partial y^2} + \bar{A}_{31}^e\psi + N_x^e,$$

$$N_y = A_{12}\frac{\partial u}{\partial x} + A_{22}\frac{\partial v}{\partial y} - B_{12}\frac{\partial^2 w_b}{\partial x^2} - B_{22}\frac{\partial^2 w_b}{\partial y^2} - B_{12}^a\frac{\partial^2 w_s}{\partial x^2} - B_{22}^a\frac{\partial^2 w_s}{\partial y^2} + \bar{A}_{32}^e\psi + N_y^e,$$

$$M_x = B_{11}\frac{\partial u}{\partial x} + B_{12}\frac{\partial v}{\partial y} - D_{11}\frac{\partial^2 w_b}{\partial x^2} - D_{12}\frac{\partial^2 w_b}{\partial y^2} - D_{11}^a\frac{\partial^2 w_s}{\partial x^2} - D_{12}^a\frac{\partial^2 w_s}{\partial y^2} + \bar{A}_{31}^{ze}\psi + M_x^e,$$

$$M_y = B_{12}\frac{\partial u}{\partial x} + B_{22}\frac{\partial v}{\partial y} - D_{12}\frac{\partial^2 w_b}{\partial x^2} - D_{22}\frac{\partial^2 w_b}{\partial y^2} - D_{12}^a\frac{\partial^2 w_s}{\partial x^2} - D_{22}^a\frac{\partial^2 w_s}{\partial y^2} + \bar{A}_{32}^{ze}\psi + M_y^e,$$

$$P_x = B_{11}^a\frac{\partial u}{\partial x} + B_{12}^a\frac{\partial v}{\partial y} - D_{11}^a\frac{\partial^2 w_b}{\partial x^2} - D_{12}^a\frac{\partial^2 w_b}{\partial y^2} - F_{11}\frac{\partial^2 w_s}{\partial x^2} - F_{12}\frac{\partial^2 w_s}{\partial y^2} + \bar{A}_{31}^{fe}\psi + P_x^e,$$

$$P_y = B_{12}^a\frac{\partial u}{\partial x} + B_{22}^a\frac{\partial v}{\partial y} - D_{12}^a\frac{\partial^2 w_b}{\partial x^2} - D_{22}^a\frac{\partial^2 w_b}{\partial y^2} - F_{12}\frac{\partial^2 w_s}{\partial x^2} - F_{22}\frac{\partial^2 w_s}{\partial y^2} + \bar{A}_{32}^{fe}\psi + P_y^e,$$

$$N_{xy} = A_{66}\left(\frac{\partial u}{\partial y} + \frac{\partial v}{\partial x}\right) - 2\left(B_{66}\frac{\partial^2 w_b}{\partial x\partial y} + B_{66}^a\frac{\partial^2 w_s}{\partial x\partial y}\right),$$

$$M_{xy} = B_{66}\left(\frac{\partial u}{\partial y} + \frac{\partial v}{\partial x}\right) - 2\left(D_{66}\frac{\partial^2 w_b}{\partial x\partial y} + D_{66}^a\frac{\partial^2 w_s}{\partial x\partial y}\right),$$

$$P_{xy} = B_{66}^a\left(\frac{\partial u}{\partial y} + \frac{\partial v}{\partial x}\right) - 2\left(D_{66}^a\frac{\partial^2 w_b}{\partial x\partial y} + F_{66}\frac{\partial^2 w_s}{\partial x\partial y}\right),$$

$$Q_{yz} = A_{44}^a\frac{\partial w_s}{\partial y} - \bar{A}_{24}^e\frac{\partial \psi}{\partial y}, \qquad Q_{xz} = A_{55}^a\frac{\partial w_s}{\partial x} - \bar{A}_{15}^e\frac{\partial \psi}{\partial x},$$

$$\tilde{D}_x = \bar{A}_{15}^e\frac{\partial w_s}{\partial x} - \bar{D}_{11}^e\frac{\partial \psi}{\partial x}, \qquad \tilde{D}_y = \bar{A}_{24}^e\frac{\partial w_s}{\partial y} - \bar{D}_{22}^e\frac{\partial \psi}{\partial y},$$

$$\tilde{D}_z = \bar{A}_{31}^e\frac{\partial u}{\partial x} - \bar{A}_{31}^{ze}\frac{\partial^2 w_b}{\partial x^2} - \bar{A}_{31}^{fe}\frac{\partial^2 w_s}{\partial x^2} + \bar{A}_{32}^e\frac{\partial v}{\partial y} - \bar{A}_{32}^{ze}\frac{\partial^2 w_b}{\partial y^2} - \bar{A}_{32}^{fe}\frac{\partial^2 w_s}{\partial y^2} + \bar{H}_{33}^e\psi - D_z^e,$$

(12)

where

$$\{A_{ij}, B_{ij}, D_{ij}, F_{ij}, A_{ij}^a, B_{ij}^a, D_{ij}^a\} = \int_{-h/2}^{h/2} c_{ij}\{1, z, z^2, f^2, g^2, f, fz\}\mathrm{d}z,$$

$$\bar{A}_{31}^{ie} = \int_{-h/2}^{h/2} e_{31}\{1, z, f(z)\}\xi\sin(\xi z)\,\mathrm{d}z, \qquad i = 1, z, f,$$

$$\bar{A}_{32}^{ie} = \int_{-h/2}^{h/2} e_{32}\{1, z, f(z)\}\xi\sin(\xi z)\,\mathrm{d}z, \qquad i = 1, z, f,$$

(13)

$$\{\bar{A}_{24}^e, \bar{A}_{15}^e\} = \int_{-h/2}^{h/2}\{e_{24}, e_{15}\}\cos^2(\xi z)\,\mathrm{d}z, \quad \bar{D}_{ii}^e = \int_{-h/2}^{h/2}\mu_{ii}\cos^2(\xi z)\,\mathrm{d}z, \qquad (i = 1,2),$$

$$\bar{H}_{33}^e = \int_{-h/2}^{h/2}\mu_{33}\xi^2\sin^2(\xi z)\,\mathrm{d}z, \quad \{N_x^e, M_x^e, P_x^e\} = \int_{-h/2}^{h/2}\frac{2\psi_0}{h}e_{31}\{1, z, f(z)\}\mathrm{d}z,$$

$$\{N_y^e, M_y^e, P_y^e\} = \int_{-h/2}^{h/2}\frac{2\psi_0}{h}e_{32}\{1, z, f(z)\}\mathrm{d}z, \quad D_z^e = \int_{-h/2}^{h/2}\mu_{33}\frac{2}{h}\psi_0\xi\sin(\xi z)\,\mathrm{d}z.$$

Using Eq. (10) and integrating by parts, the equilibrium equations related with the present theory are obtained as

$$\frac{\partial N_x}{\partial x} + \frac{\partial N_{xy}}{\partial y} = 0, \qquad \frac{\partial N_{xy}}{\partial x} + \frac{\partial N_y}{\partial y} = 0,$$

$$\frac{\partial^2 M_x}{\partial x^2} + 2\frac{\partial^2 M_{xy}}{\partial x \partial y} + \frac{\partial^2 M_y}{\partial y^2} + q = 0,$$

$$\frac{\partial^2 P_x}{\partial x^2} + 2\frac{\partial^2 P_{xy}}{\partial x \partial y} + \frac{\partial^2 P_y}{\partial y^2} + \frac{\partial Q_{xz}}{\partial x} + \frac{\partial Q_{yz}}{\partial y} + q = 0, \qquad (14)$$

$$\frac{\partial \widehat{D}_x}{\partial x} + \frac{\partial \widehat{D}_y}{\partial y} + \widehat{D}_z = 0.$$

Finally, substituting Eqs. (4) and (12) into Eq. (14) yields the equilibrium equations as

$$A_{11}\frac{\partial^2 u}{\partial x^2} + A_{66}\frac{\partial^2 u}{\partial y^2} + (A_{12} + A_{66})\frac{\partial^2 v}{\partial x \partial y} - B_{11}\frac{\partial^3 w_b}{\partial x^3} - (B_{12} + 2B_{66})\frac{\partial^3 w_b}{\partial x \partial y^2}$$

$$-B_{11}^a\frac{\partial^3 w_s}{\partial x^3} - (B_{12}^a + 2B_{66}^a)\frac{\partial^3 w_s}{\partial x \partial y^2} + \bar{A}_{31}^e\frac{\partial \psi}{\partial x} + \frac{\partial N_x^e}{\partial x} = 0,$$

$$A_{66}\frac{\partial^2 v}{\partial x^2} + A_{22}\frac{\partial^2 v}{\partial y^2} + (A_{12} + A_{66})\frac{\partial^2 u}{\partial x \partial y} - B_{22}\frac{\partial^3 w_b}{\partial y^3} - (B_{12} + 2B_{66})\frac{\partial^3 w_b}{\partial x^2 \partial y}$$

$$-B_{22}^a\frac{\partial^3 w_s}{\partial y^3} - (B_{12}^a + 2B_{66}^a)\frac{\partial^3 w_s}{\partial x^2 \partial y} + \bar{A}_{31}^e\frac{\partial \psi}{\partial y} + \frac{\partial N_y^e}{\partial y} = 0,$$

$$B_{11}\frac{\partial^3 u}{\partial x^3} + (B_{12} + 2B_{66})\left(\frac{\partial^3 u}{\partial x \partial y^2} + \frac{\partial^3 v}{\partial x^2 \partial y}\right) + B_{22}\frac{\partial^3 v}{\partial y^3} - D_{11}\frac{\partial^4 w_b}{\partial x^4} - D_{22}\frac{\partial^4 w_b}{\partial y^4}$$

$$-2(D_{12} + 2D_{66})\frac{\partial^4 w_b}{\partial x^2 \partial y^2} - D_{11}^a\frac{\partial^4 w_s}{\partial x^4} - D_{22}^a\frac{\partial^4 w_s}{\partial y^4} - 2(D_{12}^a + 2D_{66}^a)\frac{\partial^4 w_s}{\partial x^2 \partial y^2}$$

$$+q + \bar{A}_{31}^{ze}\frac{\partial^2 \psi}{\partial x^2} + \bar{A}_{32}^{ze}\frac{\partial^2 \psi}{\partial y^2} + \frac{\partial^2 M_x^e}{\partial x^2} + \frac{\partial^2 M_y^e}{\partial y^2} = 0, \qquad (15)$$

$$B_{11}^a\frac{\partial^3 u}{\partial x^3} + (B_{12}^a + 2B_{66}^a)\left(\frac{\partial^3 u}{\partial x \partial y^2} + \frac{\partial^3 v}{\partial x^2 \partial y}\right) + B_{22}^a\frac{\partial^3 v}{\partial y^3} - D_{11}^a\frac{\partial^4 w_b}{\partial x^4} - D_{22}^a\frac{\partial^4 w_b}{\partial y^4}$$

$$-2(D_{12}^a + 2D_{66}^a)\frac{\partial^4 w_b}{\partial x^2 \partial y^2} - F_{11}\frac{\partial^4 w_s}{\partial x^4} - F_{22}\frac{\partial^4 w_s}{\partial y^4} - 2(F_{12} + 2F_{66})\frac{\partial^4 w_s}{\partial x^2 \partial y^2}$$

$$+A_{55}^a\frac{\partial^2 w_s}{\partial x^2} + A_{44}^a\frac{\partial^2 w_s}{\partial y^2} + \bar{A}_{31}^{fe}\frac{\partial^2 \psi}{\partial x^2} + \bar{A}_{32}^{fe}\frac{\partial^2 \psi}{\partial y^2} - \bar{A}_{24}^e\frac{\partial^2 \psi}{\partial y^2} - \bar{A}_{15}^e\frac{\partial^2 \psi}{\partial x^2}$$

$$+q + \frac{\partial^2 P_x^e}{\partial x^2} + \frac{\partial^2 P_y^e}{\partial y^2} = 0,$$

$$\bar{A}_{15}^e\frac{\partial^2 w_s}{\partial x^2} + \bar{D}_{11}^e\frac{\partial^2 \psi}{\partial x^2} + \bar{A}_{24}^e\frac{\partial^2 w_s}{\partial y^2} + \bar{D}_{11}^e\frac{\partial^2 \psi}{\partial y^2} + \bar{A}_{31}^e\frac{\partial u}{\partial x} + \bar{A}_{32}^e\frac{\partial v}{\partial y}$$

$$-\bar{A}_{31}^{ze}\frac{\partial^2 w_b}{\partial x^2} - \bar{A}_{32}^{ze}\frac{\partial^2 w_b}{\partial y^2} - \bar{A}_{31}^{fe}\frac{\partial^2 w_s}{\partial x^2} - \bar{A}_{32}^{fe}\frac{\partial^2 w_s}{\partial x^2} + \bar{H}_{33}^e\psi - D_z^e = 0.$$

3. Exact solution

In the present study, the rectangular FGP plate is subjected to simply-supported conditions and the electric potential is zero at all edges of the plate. So, one can solve the problem analytically and the boundary conditions will be simplified as

$$
\begin{aligned}
u(x,0) &= u(x,b) = u(0,y) = u(a,y) = 0, \\
v(x,0) &= v(x,b) = v(0,y) = v(a,y) = 0, \\
w_b(x,0) &= w_b(x,b) = w_b(0,y) = w_b(a,y) = 0, \\
w_s(x,0) &= w_s(x,b) = w_s(0,y) = w_s(a,y) = 0, \\
\psi(x,0) &= \psi(x,b) = \psi(0,y) = \psi(a,y) = 0.
\end{aligned}
\tag{16}
$$

The solution to the equilibrium equations can be supposed as:

$$
\begin{Bmatrix} u \\ v \\ [w_b, w_s, \psi] \end{Bmatrix} = \begin{Bmatrix} U\cos(\lambda x)\sin(\mu y) \\ V\sin(\lambda x)\cos(\mu y) \\ [W_b, W_s, \Psi]\sin(\lambda x)\sin(\mu y) \end{Bmatrix},
\tag{17}
$$

where $\lambda = \pi/a$, $\mu = \pi/b$. and U, V, W_b, W_s, Y and Ψ are unknowns Fourier expansion coefficients. Both the mechanical load q and the applied voltage ψ_0 are applied sinusoidally on the upper surface of the FGP plate and they can be expressed as

$$
\begin{Bmatrix} q \\ \psi_0 \end{Bmatrix} = \begin{Bmatrix} q_0 \\ \tilde{\psi}_0 \end{Bmatrix} \sin(\lambda x)\sin(\mu y),
\tag{18}
$$

where q_0 is the intensity of the mechanical load and $\tilde{\psi}_0$ is the applied electric voltage. Using Eqs. (17)-(18) in Eq. (14), we get

$$
[L]\{\Delta\} = \{F\},
\tag{19}
$$

where $\{\Delta\} = \{U, V, W_b, W_s, \Psi\}^T$ and the component of the vector force $\{F\}$ are given by

$$
\begin{aligned}
F_1 &= \frac{\partial N_x^e}{\partial x}, \qquad F_2 = \frac{\partial N_y^e}{\partial y}, \\
F_3 &= q_0 + \frac{\partial^2 M_x^e}{\partial x^2} + \frac{\partial^2 M_y^e}{\partial y^2}, \\
F_4 &= q_0 + \frac{\partial^2 P_x^e}{\partial x^2} + \frac{\partial^2 P_y^e}{\partial y^2}, \qquad F_5 = D_z^e,
\end{aligned}
\tag{20}
$$

and L_{ij} represent the coefficients of the symmetric stiffness matrix $[L]$ which are given by

$$
\begin{aligned}
L_{11} &= A_{11}\lambda^2 + A_{66}\mu^2, \qquad L_{12} = (A_{12} + A_{66})\lambda\mu, \qquad L_{13} = -B_{11}\lambda^3 - (B_{12} + 2B_{66})\lambda\mu^2, \\
L_{14} &= -B_{11}^a\lambda^3 - (B_{12}^a + 2B_{66}^a)\lambda\mu^2, \qquad L_{15} = -\bar{A}_{31}^e\lambda, \qquad L_{22} = A_{66}\lambda^2 + A_{22}\mu^2, \\
L_{23} &= -B_{22}\mu^3 - (B_{12} + 2B_{66})\lambda^2\mu, \qquad L_{24} = -B_{22}^a\mu^3 - (B_{12}^a + 2B_{66}^a)\lambda^2\mu, \qquad L_{25} = -\bar{A}_{32}^e\mu, \\
L_{33} &= D_{11}\lambda^4 + 2(D_{12} + 2D_{66})\lambda^2\mu^2 + D_{22}\mu^4, \qquad L_{34} = D_{11}^a\lambda^4 + 2(D_{12}^a + 2D_{66}^a)\lambda^2\mu^2 + D_{22}^a\mu^4, \\
L_{35} &= \bar{A}_{31}^{ze}\lambda^2 + \bar{A}_{32}^{ze}\mu^2, \qquad L_{44} = F_{11}\lambda^4 + 2(F_{12} + 2F_{66})\lambda^2\mu^2 + F_{22}\mu^4 + A_{55}^a\lambda^2 + A_{44}^a\mu^2, \\
L_{45} &= \bar{A}_{31}^{fe}\lambda + \bar{A}_{15}^e\lambda^2 + \bar{A}_{32}^{fe}\mu + \bar{A}_{24}^e\mu^2, \qquad L_{55} = \bar{D}_{11}^e(\lambda^2 + \mu^2) + \bar{H}_{33}^e.
\end{aligned}
\tag{21}
$$

Table 1 The deflection and normal stress in the FGP square plate

k	Methods		$\overline{w}(0)$			$\overline{\sigma}_x(1/3)$		
			$a/h = 4$	$a/h = 10$	$a/h = 100$	$a/h = 4$	$a/h = 10$	$a/h = 100$
1	CPT (Carrera *et al.* 2008)		0.5623	0.5623	0.5623	0.8060	2.0150	20.150
	FSDT (Carrera *et al.* 2008)		0.7291	0.5889	0.5625	0.8060	2.0150	20.150
	Q-3D (Carrera *et al.* 2008)		0.7171	0.5875	0.5625	0.6221	1.5064	14.969
	Q-3D (Carrera *et al.* 2011)		0.7171	0.5875	0.5625	0.6221	1.5064	14.969
	Present	FG	0.7284	0.5889	0.5625	0.5812	1.4898	14.967
		FGP ($\psi_0 = 0.5$)	-0.0305	0.0354	0.0005	0.1835	1.8186	21.612
		FGP ($\psi_0 = 0$)	0.1271	0.0442	0.0005	0.7731	2.0844	21.640
		FGP ($\psi_0 = -0.5$)	2.8498	0.5303	0.0056	1.3635	2.3504	21.669
4	CPT (Carrera *et al.* 2008)		0.8281	0.8281	0.8281	0.6420	1.6049	16.049
	FSDT (Carrera *et al.* 2008)		1.1125	0.8736	0.8286	0.6420	1.6049	16.049
	Q-3D (Carrera *et al.* 2008)		1.1585	0.8821	0.8286	0.4877	1.1971	11.923
	Q-3D (Carrera *et al.* 2011)		1.1585	0.8821	0.8286	0.4877	1.1971	11.923
	Present	FG	1.1598	0.8815	0.8287	0.4449	1.1793	11.921
		FGP ($\psi_0 = 0.5$)	-0.1446	0.0625	0.0011	0.2052	1.7468	21.598
		FGP ($\psi_0 = 0$)	0.2129	0.0854	0.0011	0.7128	2.0114	21.629
		FGP ($\psi_0 = -0.5$)	5.7046	1.0846	0.0119	1.2206	2.2760	21.659
10	CPT (Carrera *et al.* 2008)		0.9354	0.9354	0.9354	0.4796	1.1990	11.990
	FSDT (Carrera *et al.* 2008)		1.3178	0.9966	0.9360	0.4796	1.1990	11.990
	Q-3D (Carrera *et al.* 2008)		1.3745	1.0072	0.9361	0.3695	0.8965	8.6077
	Q-3D (Carrera *et al.* 2011)		1.3745	1.0072	0.9361	0.3695	0.8965	8.6077
	Present	FG	1.3908	1.0087	0.9362	0.3258	0.8784	8.9060
		FGP ($\psi_0 = 0.5$)	-0.0657	0.0892	0.0016	-0.0086	1.6003	21.576
		FGP ($\psi_0 = 0$)	0.2551	0.1117	0.0016	0.6460	1.9243	21.614
		FGP ($\psi_0 = -0.5$)	5.7607	1.3424	0.0166	1.3011	2.2483	21.651

4. Numerical results and discussions

In this part, the numerical results are presented for simply-supported FGP rectangular plates. The material properties of the FGP plate made of metal (Aluminum, Al) and ceramic (Alumina, $Al_2 O_3$) are given by

$$E_m = 70 \text{ GPa}, \qquad E_c = 380 \text{ GPa}, \qquad \nu = 0.3. \qquad (22)$$

Before submitting the numerical results, a comparison is made with previous works to validate the present formulation. Table 1 shows the calculated results of non-dimensional displacement $\overline{w}$ and stress $\overline{\sigma}_x$ of the square FGP plate under sinusoidal load as compared with the published results by Carrera *et al.* (2008, 2011). The results presented in the papers of Mantari *et al.* (2012c), Zenkour (2006) and Carrera *et al.* (2011) are also taken as references and used for the validation purposes in Table 2.

The non-dimensional form of the deflection and stress parameters of mechanical bending are

$$\overline{w} = \frac{10h^3 E_c}{a^4 q_0} w\left(\frac{a}{2}, \frac{b}{2}, \overline{z}\right), \qquad \overline{\sigma}_i = \frac{h}{a q_0} \sigma_i\left(\frac{a}{2}, \frac{b}{2}, \overline{z}\right), \qquad (i = x, y),$$

$$\overline{\tau}_{xy} = \frac{h}{a q_0} \tau_{xy}(0,0,\overline{z}), \qquad \overline{\tau}_{yz} = \frac{h}{a q_0} \tau_{yz}\left(\frac{a}{2}, 0, \overline{z}\right), \qquad (23)$$

$$\overline{\tau}_{xz} = \frac{h}{aq_0}\tau_{xz}\left(0,\frac{b}{2},\overline{z}\right), \overline{\psi} = \frac{10^3 h^3}{a^2 q_0}\frac{e_{31}}{}\psi\left(\frac{a}{2},\frac{b}{2},\overline{z}\right),$$

$$\overline{D}_z = \frac{h^3 E_c}{a^2 q_0\ e_{31}}D_z\left(\frac{a}{2},\frac{b}{2},\overline{z}\right), \qquad \overline{z} = \frac{z}{h}, \qquad \tilde{\psi}_0 = \frac{\psi_0}{hq_0}\ . \tag{23}$$

The present results are compared well with those of Carrera *et al.* (2008, 2011) in Table 1 and with those of Mantari *et al.* (2012c), Zenkour (2006) and Carrera *et al.* (2011) in Table 2. In fact, some further results are also reported in Tables 1 and 2 for the FGP plates to observe the impact of the external electric voltage $\tilde{\psi}_0$. We use the values of $\tilde{\psi}_0 = -0.5,\ 0$ and 0.5 for this purpose. It is clear that, in both tables the value of $\tilde{\psi}_0 = -0.5$ gives the largest deflection while $\tilde{\psi}_0 = 0.5$ gives the smallest one. Table 1 shows that the deflection $\overline{w}$ decreases as k decreases and a/h, $\tilde{\psi}_0$ increases while the normal stress $\overline{\sigma}_x$ increases as a/h, k increases and $\tilde{\psi}_0$ decreases. Table 2 illustrates that the dimensionless deflection $\overline{w}$ and stresses $\overline{\tau}_{xy}$, $\overline{\tau}_{xz}$ increase as $\tilde{\psi}_0$ decreases and k increases. In the same table the normal stress $\overline{\sigma}_x$ decreases as k increases and $\tilde{\psi}_0$ decreases.

Table 2 The deflection and stresses in the FGP square plate at $a/h = 10$

| k	Methods		$\overline{w}(0)$	$\overline{\sigma}_x(1/3)$	$\overline{\tau}_{xy}(-1/3)$	$\overline{\tau}_{xz}(1/6)$
	Q-3D (Carrera *et al.* 2008)		0.5875	1.5062	0.6081	0.2510
	SSDT (Zenkour, 2006)		0.5889	1.4894	0.6110	0.2622
	HSDT (Mantari *et al.* 2012c)		0.5880	1.4888	0.6109	0.2566
1		FG	0.5889	1.4898	0.6111	0.2607
	Present	FGP ($\psi_0 = 0.5$)	0.0354	1.8186	-0.3206	0.1730
		FGP ($\psi_0 = 0$)	0.0442	2.0844	0.8278	0.1626
		FGP ($\psi_0 = -0.5$)	0.5303	2.3504	1.9763	0.1523
	Q-3D (Carrera *et al.* 2008)		0.7570	1.4147	0.5421	0.2496
	SSDT (Zenkour 2006)		0.7573	1.3954	0.5441	0.2763
	HSDT (Mantari *et al.* 2012c)		0.7564	1.3940	0.5438	0.2741
2		FG	0.7573	1.3960	0.5442	0.2736
	Present	FGP ($\psi_0 = 0.5$)	0.0456	1.7977	-0.2323	0.1624
		FGP ($\psi_0 = 0$)	0.0614	2.0674	0.7989	0.1443
		FGP ($\psi_0 = -0.5$)	0.7734	2.3372	1.8302	0.1261
	Q-3D (Carrera *et al.* 2008)		0.8823	1.1985	0.5666	0.2362
	SSDT (Zenkour 2006)		0.8819	1.1783	0.5667	0.2580
	HSDT (Mantari *et al.* 2012c)		0.8814	1.1755	0.5662	0.2623
4		FG	0.8815	1.1793	0.5669	0.2536
	Present	FGP ($\psi_0 = 0.5$)	0.0625	1.7468	-0.2332	0.1789
		FGP ($\psi_0 = 0$)	0.0854	2.0114	1.0053	0.1665
		FGP ($\psi_0 = -0.5$)	1.0846	2.2760	2.2438	0.1541
	Q-3D (Carrera *et al.* 2008)		0.9738	0.9687	0.5879	0.2262
	SSDT (Zenkour 2006)		0.9750	0.9466	0.5856	0.2121
	HSDT (Mantari *et al.* 2012c)		0.9737	0.9431	0.5850	0.2140
8		FG	0.9746	0.9476	0.5858	0.2087
	Present	FGP ($\psi_0 = 0.5$)	0.0829	1.6385	-0.2993	0.2119
		FGP ($\psi_0 = 0$)	0.1067	1.9420	1.1848	0.2130
		FGP ($\psi_0 = -0.5$)	1.3057	2.2455	2.6690	0.2142
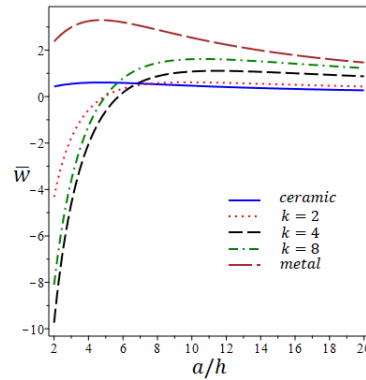
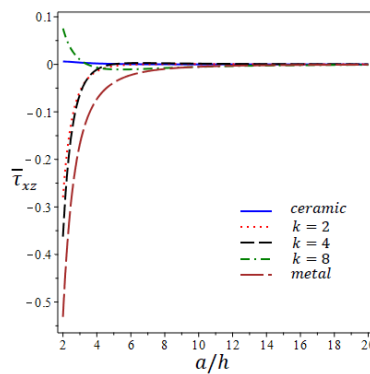Fig. 2 Variation of the deflection $\overline{w}$ vs the thickness ratio a/h

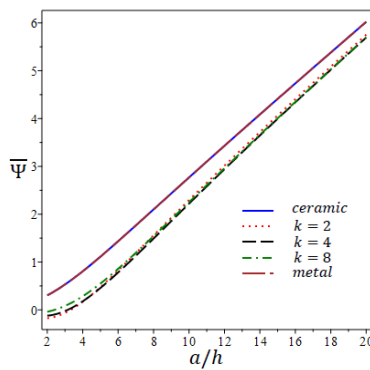Fig. 3 Variation of the transverse shear stress $\overline{\tau}_{xz}$ vs the thickness ratio a/h

Fig. 4 Variation of the electric potential $\overline{\Psi}$ vs the thickness ratio a/h

Figs. 2 and 3 illustrate the variation of the deflection $\overline{w}$ and the transverse shear stress $\overline{\tau}_{xz}$ versus the thickness ratio a/h ($a/b = 1$, $\tilde{\psi}_0 = 1$). According to Fig. 2, the deflection $\overline{w}$ increases as a/h increases and k decreases for the FGP plate only while the deflections $\overline{w}$ for the homogeneous ceramic and metal plates is decreasing as a/h increases. Also, in Fig. 3 the transverse shear stress $\overline{\tau}_{xz}$ is increasing with the increases in the thickness of the square plate,
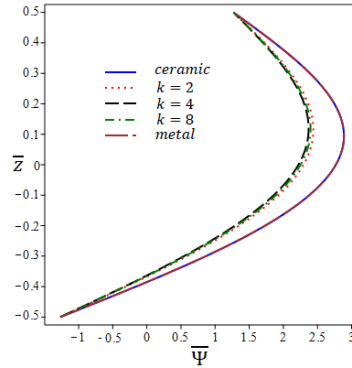
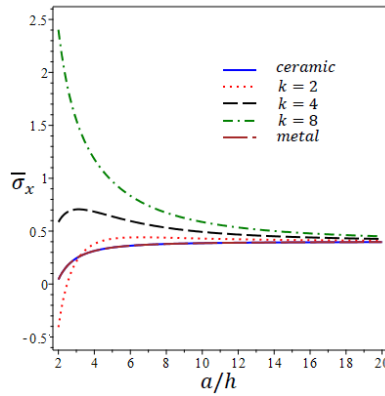Fig. 5 Variation of the electric potential $\overline{\Psi}$ through-the-thickness of the FGP plate

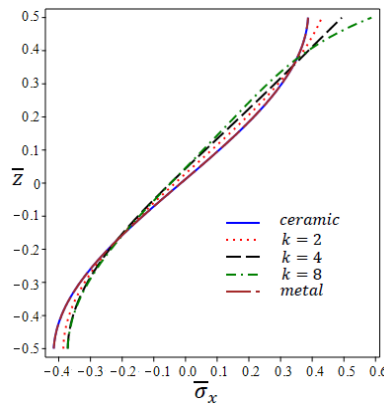Fig. 6 Variation of the normal stress $\overline{\sigma}_x$ vs the thickness ratio a/h

Fig. 7 Variation of the normal stress $\overline{\sigma}_x$ through-the-thickness of the FGP plate

especially for small values of a/h. It will be independent of the variation in a/h with the increase of thickness ratio.

Figs. 4 and 5 demonstrate the variation of the electric potential $\overline{\Psi}$ versus the thickness ratio a/h and through-the-thickness of the FGP square plate ($a/h = 10$, $\tilde{\psi}_0 = 1$). As per in Fig. 4, the
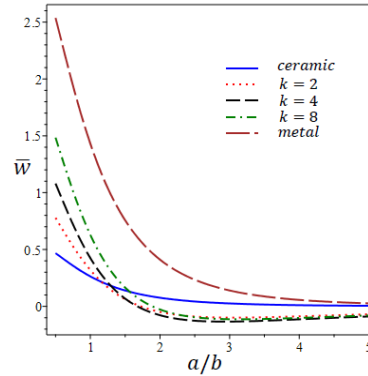
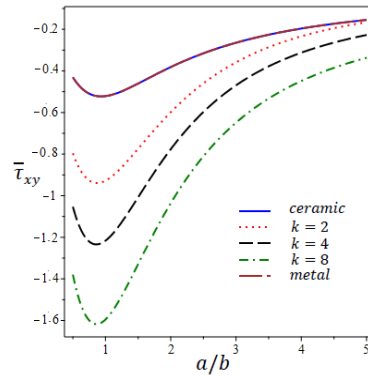Fig. 8 Variation of the deflection $\overline{w}$ vs the aspect ratio a/b

Fig. 9 Variation of the transverse shear stress $\overline{\tau}_{xy}$ vs the aspect ratio a/b

electric potential $\overline{\Psi}$ increases directly as a/h increases for homogeneous and FG piezoelectric plates. The gradient index k desn't have impact on the electric potential $\overline{\Psi}$ as appeared in both figures. Also, the values of $\overline{\Psi}$ for the homogeneous ceramic and metal plates are identical.

Figs. 6 and 7 show the variation of the in-plane normal stress $\overline{\sigma}_x$ versus the thickness ratio a/h and through-the-thickness of the FGP square plate ($a/h = 10$, $\tilde{\psi}_0 = 1$). The normal stress $\overline{\sigma}_x$ increases as k increases as shown in Fig. 6. From Fig. 7 the normal stress $\overline{\sigma}_x$ is compressive in the lower half plane of the FGP plate and tensile in the upper one. Once again, the values of $\overline{\sigma}_x$ for the homogeneous ceramic and metal plates are identical.

The variation of the deflection $\overline{w}$ and transverse shear stress $\overline{\tau}_{xy}$ versus the aspect ratio a/b are shown, respectively, in Figs. 8 and 9. It can be detected from Fig. 8 that the deflection $\overline{w}$ decreases as a/b increases and k decreases for the FGP plate. The deflection of metallic plate is greater than that of the ceramic plate. From Fig. 9 the transverse shear stress $\overline{\tau}_{xy}$ is no longer decreasing as a/b increases to get its smaller values when then $a/b = 0.85$ then it increases with the increase in a/b ratio. Also, $\overline{\tau}_{xy}$ is increasing as k decreases for the FGP plate. Once again, the values of $\overline{\tau}_{xy}$ for the homogeneous ceramic and metal plates are the higher and identical.

Fig. 10 shows the variation of electric displacement $\overline{D}_z$ versus the aspect ratio a/b of the
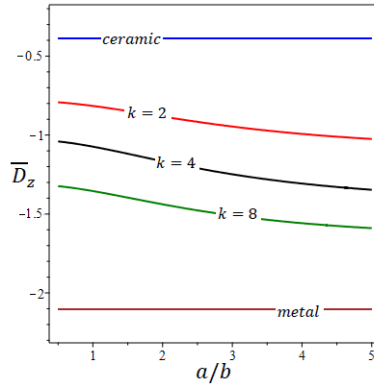
Fig. 10 Variation of the electric displacement $\overline{D}_z$ vs the aspect ratio a/b
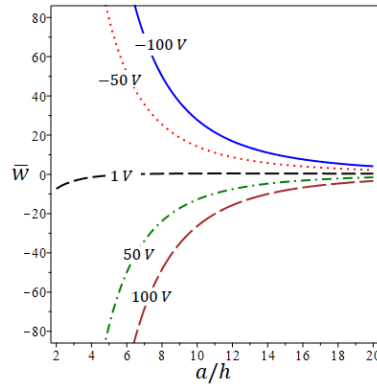

Fig. 11 Variation of the non-dimensional deflection $\overline{w}$ vs the thickness ratio a/h
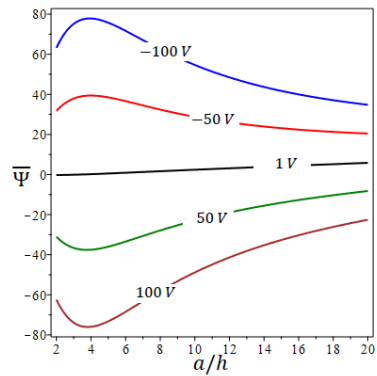

Fig. 12 Variation of the electric potential $\overline{\Psi}$ vs the thickness ratio a/h

FGP plate. The electric displacement decreases as a/b and k increase for the FGP plates while the electric displacement is linear for homogeneous (ceramic/metal) plates.

Now, one can discuss the impact and variation of the external electric voltage $\tilde{\psi}_0$ at, for example, $k = 3$. Figs. 11-17 display the variation of $\overline{w}$, $\overline{\Psi}$, $\overline{\sigma}_x$ and $\overline{\sigma}_y$, respectively, with the
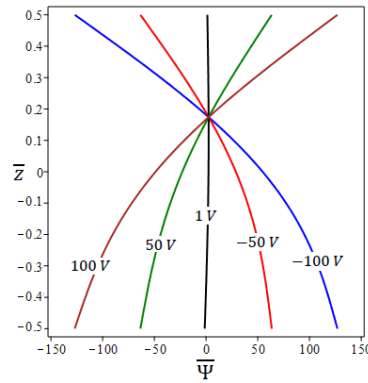
Fig. 13 Variation of the electric potential $\overline{\Psi}$ through-the-thickness of the FGP plate
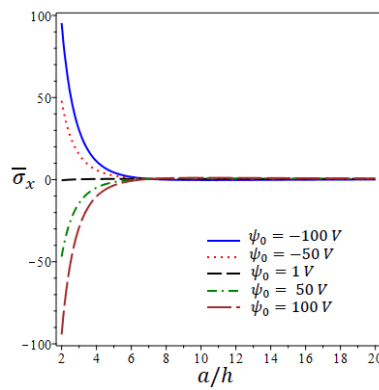

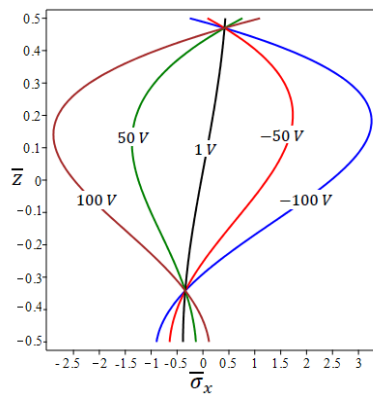Fig. 14 Variation of the normal stress $\overline{\sigma}_x$ vs the thickness ratio a/h

Fig. 15 Variation of the normal stress $\overline{\sigma}_x$ through-the-thickness of the FGP plate

thickness ratio a/h and through-the-thickness of the FGP square plate for different value of the external electric voltage $\tilde{\psi}_0$. Fig. 11 shows the variation of the non-dimensional deflection $\overline{w}$ versus the side-to-thickness ratio of the FGP plate. Accordingly, the deflection $\overline{w}$ increases as $\tilde{\psi}_0$ decreases. Also, as a/h increases the deflection $\overline{w}$ increases for positive values of $\tilde{\psi}_0$ while it
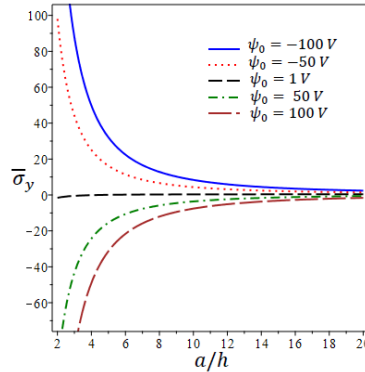
Fig. 16 Variation of the longitudinal stress $\overline{\sigma}_y$ vs the thickness ratio a/h
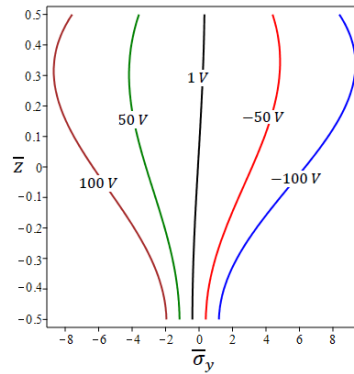

Fig. 17 Variation of the longitudinal stress $\overline{\sigma}_y$ through-the-thickness of the FGP plate

decreases for negative values of $\tilde{\psi}_0$.

Figs. 12 and 13 illustrate that the electric potential increases with the decrease in $\tilde{\psi}_0$. The electric potential $\overline{\Psi}$ may be vanished when $\tilde{\psi}_0 = 1$ V. For positive values of $\tilde{\psi}_0$ (50 V and 100 V) the electric potential $\overline{\Psi}$ is no longer decreasing as a/h increases and has its minimum values when $a/h = 3.5$ as shown in Fig. 12. Also, for negative values of $\tilde{\psi}_0$ (-50 V and -100 V) the electric potential $\overline{\Psi}$ is no longer increasing as a/h increases and has its maximum values when $a/h = 3.5$. However, Figure 13 shows that the electric potential $\overline{\Psi}$ is tensile upwards of $\bar{z} = 0.18$ for positive values of $\tilde{\psi}_0$ and downwards of $\bar{z} = 0.18$ for negative values of $\tilde{\psi}_0$. Otherwise, the electric potential $\overline{\Psi}$ is compressive upwards of $\bar{z} = 0.18$ for negative values of $\tilde{\psi}_0$ and downwards of $\bar{z} = 0.18$ for positive values of $\tilde{\psi}_0$.

Fig. 14 shows the variation of normal stress $\overline{\sigma}_x$ versus the aspect ratio a/h of the FGP plate. It is clear that, $\overline{\sigma}_x$ increases as the applied voltage $\tilde{\psi}_0$ decreases. For lower values of a/h, $\overline{\sigma}_x$ increases for positive values of $\tilde{\psi}_0$ and decreases for negative values of $\tilde{\psi}_0$. However, the normal stress $\overline{\sigma}_x$ is plotted through-the-thickness of the FGP plate in Fig. 15. It may be tensile for -ve $\tilde{\psi}_0$ and compressive for +ve $\tilde{\psi}_0$. It is obvious that the variation of $\tilde{\psi}_0$ has no effect on the normal stress $\overline{\sigma}_x$ in two positions $\bar{z} = -0.35$ and $\bar{z} = 0.45$, respectively.

Finally, Figs. 16 and 17 show the variation of the longitudinal stress $\overline{\sigma}_y$ versus the thickness

ratio and through-the-thickness of the FGP plate. Once again, $\overline{\sigma}_y$ is generally increasing as $\tilde{\psi}_0$ decreases. Also, $\overline{\sigma}_y$ increases as a/h increases for +ve $\tilde{\psi}_0$ and decreases as a/h increases for -ve $\tilde{\psi}_0$. Both figures show that the longitudinal stress is tensile for -ve $\tilde{\psi}_0$ and compressive for +ve $\tilde{\psi}_0$.

5. Conclusions

This article presents the bending analyses of the FGP plates employing a simple two-variable shear deformation plate theory. This theory contains the impacts of both shear and normal deformations and effects of thickness stretching in the FGP plate. According to the five-unknown primary variables (four mechanical displacements and one electric potential), the theory satisfies the boundary conditions on the surfaces of the FGP plate without employing shear correction factors.

The governing equations in the current study are construed based on the virtual work principle and the FGP plates analytical solutions are obtained by using the Navier's method. Numerical results due to the influences of external electric voltages and power-law indices are investigated. Moreover, the positive values of external electric voltage generate smaller values of all variables compared to negative voltages. The effect of material gradient index, plate's aspect ratio, and thickness ratio on the mechanical bending of FGP plates is also investigated. Such investigation connotes that the study can yield precise results in comparison with other theories. Therefore, it is worthy of special attention and additional enforcement by employing numerical methods.

The current study for indicates the following:

• The deflection of FGP decreases as aspect ratio increases and the gradient index decreases, while the deflection decreases as the aspect ratio increases for the FGP plate.

• The deflection of the full ceramic and full metal FGP decreases as the thickness ratio increases.

• The negative electric voltage gives the largest deflection while the positive electric voltage gives the smallest one.

• The deflection of FGP increases as the thickness ratio and electric voltage increase.

• The normal stress $\overline{\sigma}_x$ in FGP increases as the thickness ratio and gradient index increase and electric voltage decreases.

• The electric potential of FGP increases directly as the thickness ratio increases.

References

Arefi, M. and Zenkour, A.M. (2016a), "A simplified shear and normal deformations nonlocal theory for bending of functionally graded piezomagnetic sandwich nanobeams in magnet-thermo-electric environment", *J. Sandw. Struct. Mater.*, **18**, 624-651. https://doi.org/10.1177%2F1099636216652581.

Arefi, M. and Zenkour, A.M. (2016b), "Employing sinusoidal shear deformation plate theory for transient analysis of three layers sandwich nanoplate integrated with piezo-magnetic face-sheets", *Smart. Mater. Struct.*, **25**, 115040. https://doi.org/10.1088/0964-1726/25/11/115040.

Arefi, M. and Zenkour, A.M. (2017a), "Nonlocal electro-thermo mechanical analysis of a sandwich nanoplate containing a Kelvin-Voigt viscoelastic nanoplate and two piezoelectric layers", *Acta. Mech.*, **228**, 475-493. https://doi.org/10.1007/s00707-016-1716-0.

Arefi, M. and Zenkour, A.M. (2017b), "Vibration and bending analysis of a sandwich microbeam with two

integrated piezo-magnetic face sheets", *Compos. Struct.*, **159**, 479-90.
https://doi.org/10.1016/j.compstruct.2016.09.088.

Arefi, M. and Zenkour, A.M. (2017c), "Thermo-electro-mechanical bending behavior of sandwich nanoplate integrated with piezoelectric face-sheets based on trigonometric plate theory", *Compos. Struct.*, **162**, 108-22. https://doi.org/10.1016/j.compstruct.2016.11.071.

Baltacioglu, A.K., Akgoz, B. and Civalek, O. (2010), "Nonlinear static response of laminated composite plates by discrete singular convolution method", *Compos. Struct.*, **93**, 153-161. https://doi.org/10.1016/j.compstruct.2010.06.005.

Benbakhti A., Bouiadjra, M.B., Retiel, N. and Tounsi, A. (2016), "A new five unknown quasi-3D type HSDT for thermomechanical bending analysis of FGM sandwich plates", *Steel Compos. Struct.*, **22**(5), 975-999. https://doi.org/10.12989/scs.2016.22.5.975.

Bouazza, M., Zenkour, A.M. and Benseddiq, N. (2018), "Closed-from solutions for thermal buckling analyses of advanced nanoplates according to a hyperbolic four-variable refined theory with small-scale effects", *Acta Mech.*, **229**(5), 2251-2265. https://doi.org/10.1007/s00707-017-2097-8.

Carrera, E., Brischetto, S. and Robaldo, A. (2008), "Variable kinematic model for the analysis of functionally graded material plates", *AIAA J.*, **46**(1), 194-203. https://doi.org/10.2514/1.32490.

Carrera, E., Brischetto, S., Cinefra, M. and Soave, M. (2011), "Effects of thickness stretching in functionally graded plates and shells", *Compos. B Eng.*, **42**(2), 123-133.
https://doi.org/10.1016/j.compositesb.2010.10.005.

Chi, S.H. and Chung, Y.L. (2006), "Mechanical behavior of functionally graded material plates under transverse load-Part I: Analysis", *Int. J. Solid Struct.*, **43**, 3657-3674.
https://doi.org/10.1016/j.ijsolstr.2005.04.011.

Demir, C., Mercan, K. and Civalek, O. (2016), "Determination of critical buckling loads of isotropic, FGM and laminated truncated conical panel", *Compos. B Eng.*, **94**, 1-10.
https://doi.org/10.1016/j.compositesb.2016.03.031.

Ebrahimi, F. and Rastgoo, A. (2008), "Free vibration analysis of smart annular FGM plates integrated with piezoelectric layers", *Smart Mater. Struct.*, **17**(1), 15044. https://doi.org/10.1088/0964-1726/17/1/015044.

Fereidoon, A., Asghardokht, S.M. and Mohyeddin, A. (2011), "Bending analysis of thin functionally graded plates using generalized differential quadrature method", *Arch. Appl. Mech.*, **81**, 1523-1539.
https://doi.org/10.1007/s00419-010-0499-3.

Ferreira, A.J.M., Carrera, E., Cinefra, M., Roque, C.M.C. and Polit, O. (2011), "Analysis of laminated shells by a sinusoidal shear deformation theory and radial basis functions collocation, accounting for through-the-thickness deformations", *Compos. B Eng.*, **42**(5), 1276-1284.
https://doi.org/10.1016/j.compositesb.2011.01.031.

Ghasemabadian, M.A. and Kadkhodayan, M. (2016), "Investigation of buckling behavior of functionally graded piezoelectric (FGP) rectangular plates under open and closed circuit conditions", *Struct. Eng. Mech.*, **60**(2), 271-299. http://doi.org/10.12989/sem.2016.60.2.271.

Giannakopoulos, A.E. and Suresh, S. (1999), "Theory of indentation of piezoelectric materials", *Acta Mater.*, **47**, 2153-2164. https://doi.org/10.1016/S1359-6454(99)00076-2.

Gürses, M., Civalek, O., Korkmaz, A. and Ersoy, H. (2009), "Free vibration analysis of symmetric laminated skew plates by discrete singular convolution technique based on first order shear deformation theory", *Int. J. Numer. Meth. Eng.*, **79**, 290-313. https://doi.org/10.1002/nme.2553.

Jandaghian, A.A. and Rahmani, O. (2017), "Size-dependent free vibration analysis of functionally graded piezoelectric plate subjected to thermo-electro-mechanical loading", *J. Intell. Mater. Syst. Struct.*, **28**, 3039-3053. https://doi.org/10.1177%2F1045389X17704920.

Jha, D.K., Kant, T. and Singh, R.K. (2013), "A critical review of recent research on functionally graded plates", *Compos. Struct.*, **96**, 833-849. https://doi.org/10.1016/j.compstruct.2012.09.001.

Liew, K.M., He, X.Q., Tan, M.J. and Lim, H.K. (2004), "Dynamic analysis of laminated composite plates with piezoelectric sensor/actuator patches using the FSDT mesh-free method", *Int. J. Mech. Sci.*, **46**, 411-31. https://doi.org/10.1016/j.ijmecsci.2004.03.011.

Mantari, J.L. and Guedes Soares, C. (2012), "Generalized hybrid quasi-3D shear deformation theory for the

static analysis of advanced composite plates", *Compos. Struct.*, **94**(8), 2561-2575. https://doi.org/10.1016/j.compstruct.2012.02.019.

Mantari, J.L., Oktem, A.S. and Guedes Soares, C. (2012a), "A new higher order shear deformation theory for sandwich and composite laminated plates", *Compos. B Eng.*, **43**(3), 1489-1499. https://doi.org/10.1016/j.compositesb.2011.07.017.

Mantari, J.L., Oktem, A.S. and Guedes Soares, C. (2012b), "A new trigonometric shear deformation theory for isotropic, laminated composite and sandwich plates", *Int. J. Solids Struct.*, **49**(1), 43-53. https://doi.org/10.1016/j.ijsolstr.2011.09.008.

Mantari, J.L., Oktem, A.S. and Guedes Soares, C. (2012c), "Bending response of functionally graded plates by using a new higher order shear deformation theory", *Compos. Struct.*, **94**(2), 714-723. https://doi.org/10.1016/j.compstruct.2011.09.007.

Matsunaga, H. (2009), "Stress analysis of functionally graded plates subjected to thermal and mechanical loadings", *Compos. Struct.*, **87**, 344-357. https://doi.org/10.1016/j.compstruct.2008.02.002.

Mindlin, R.D. (1951), "Influence of rotatory inertia and shear on flexural motions of isotropic elastic plates", *ASME J. Appl. Mech.*, **18**, 31-38.

Neves, A.M.A., Ferreira, A.J.M., Carrera, E., Cinefra, M., Roque, C.M.C., Jorge, R.M.N. and Soares, C.M.M. (2012a), "A quasi-3D hyperbolic shear deformation theory for the static and free vibration analysis of functionally graded plates", *Compos. Struct.*, **94**(5), 1814-1825. https://doi.org/10.1016/j.compstruct.2011.12.005.

Neves, A.M.A., Ferreira, A.J.M., Carrera, E., Roque, C.M.C., Cinefra, M., Jorge, R.M.N. and Soares, C.M.M. (2012b), "A quasi-3D sinusoidal shear deformation theory for the static and free vibration analysis of functionally graded plates", *Compos. B Eng.*, **43**(2), 711-725. https://doi.org/10.1016/j.compositesb.2011.08.009.

Neves, A.M.A., Ferreira, A.J.M., Carrera, E., Cinefra, M., Roque, C.M.C., Jorge, R.M.N. and Soares, C.M. (2013) "Static, free vibration and buckling analysis of isotropic and sandwich functionally graded plates using a quasi-3D higher-order shear deformation theory and a meshless technique", *Compos. B Eng.*, **44**(1), 657-674. https://doi.org/10.1016/j.compositesb.2012.01.089.

Pradyumna, S. and Bandyopadhyay, J.N. (2008), "Free vibration analysis of functionally graded curved panels using a higher-order finite element formulation", *J. Sound Vib.*, **318**(1-2), 176-192. https://doi.org/10.1016/j.jsv.2008.03.056.

Reddy, J.N. (1984), "A simple higher-order theory for laminated composite plates", *J. Appl. Mech.*, **51**, 745-52. https://doi.org/10.1115/1.3167719.

Reddy, J.N. (2000), "Analysis of functionally graded plates", *Int. J. Numer. Meth. Eng.*, **47**(1-3), 663-684. https://doi.org/10.1002/(SICI)1097-0207(20000110/30)47:1/3%3C663::AID-NME787%3E3.0.CO;2-8.

Reddy, J.N. (2011), "A general nonlinear third-order theory of functionally graded plates", *Int. J. Aerosp. Lightweight Struct.*, **1**(1), 1-21. http://dx.doi.org/10.3850/S201042861100002X.

Reissner, E. (1944), "On the theory of bending of elastic plates", *J. Math. Phys.*, **23**, 184-191. https://doi.org/10.1002/sapm1944231184.

Reissner, E. (1945), "The effect of transverse shear deformation on the bending of elastic plates", *J. Appl. Mech.*, **12**, 69-77.

Talha, M. and Singh, B.N. (2010), "Static response and free vibration analysis of FGM plates using higher order shear deformation theory", *Appl. Math. Model.*, **34**(12), 3991-4011. https://doi.org/10.1016/j.apm.2010.03.034.

Tu, T.M., Quoc, T.H. and Long, N.V. (2017), "Bending analysis of functionally graded plates using new eight-unknown higher order shear deformation theory", *Struct. Eng. Mech.*, **62**(3), 311-324. https://doi.org/10.12989/sem.2017.62.3.311.

Zenkour, A.M. (2004), "Thermal effects on the bending response of fiber-reinforced viscoelastic composite plates using a sinusoidal shear deformation theory", *Acta Mech.*, **171**(3-4), 171-187. https://doi.org/10.1007/s00707-004-0145-7.

Zenkour, A.M. (2005a), "A comprehensive analysis of functionally graded sandwich plates: Part 1—Deflection and stresses", *Int. J. Solids Struct.*, **42**(18-19), 5224-5242.

https://doi.org/10.1016/j.ijsolstr.2005.02.015.

Zenkour, A.M. (2005b), "A comprehensive analysis of functionally graded sandwich plates: Part 2—Buckling and free vibration", *Int. J. Solids Struct.*, **42**(18-19), 5243-5258. https://doi.org/10.1016/j.ijsolstr.2005.02.016.

Zenkour, A.M. (2005c), "On vibration of functionally graded plates according to a refined trigonometric plate theory", *Int. J. Struct. Stab. Dyn.*, **5**(2), 279-297. https://doi.org/10.1142/S0219455405001581.

Zenkour, A.M. (2006), "Generalized shear deformation theory for bending analysis of functionally graded plates", *Appl. Math. Model.*, **30**(1), 67-84. https://doi.org/10.1016/j.apm.2005.03.009.

Zenkour, A.M. (2007), "Benchmark trigonometric and 3-D elasticity solutions for an exponentially graded thick rectangular plate", *Arch. Appl. Mech.*, **77**(4), 197-214. https://doi.org/10.1007/s00419-006-0084-y.

Zenkour, A.M. (2009), "The refined sinusoidal theory for FGM plates on elastic foundations", *Int. J. Mech. Sci.*, **51**(11-12), 869-880. https://doi.org/10.1016/j.ijmecsci.2009.09.026.

Zenkour, A.M. (2013a), "A simple four-unknown refined theory for bending analysis of functionally graded plates", *Appl. Math. Model.*, **37**(20-21), 9041-9051. https://doi.org/10.1016/j.apm.2013.04.022.

Zenkour, A.M. (2013b), "Bending analysis of functionally graded sandwich plates using a simple four-unknown shear and normal deformations theory", *J. Sandw. Struct. Mater.*, **15**(6), 629-656. https://doi.org/10.1177%2F1099636213498886.

Zenkour, A.M. (2013c), "Bending of FGM plates by a simplified four-unknown shear and normal deformations theory", *Int. J. Appl. Mech.*, **5**(2) 1350020, 1-15. https://doi.org/10.1142/S1758825113500208.

Zenkour, A.M. (2015), "Thermal bending of layered composite plates resting on elastic foundations using four-unknown shear and normal deformations theory", *Compos. Struct.*, **122**, 260-270. https://doi.org/10.1016/j.compstruct.2014.11.064.

Zenkour, A.M. and Aljadani, M.H. (2018), "Mechanical buckling of functionally graded plates using a refined higher-order shear and normal deformation plate theory", *Adv. Aircraft Spacecraft Sci.*, **5**(6), 615-632. https://doi.org/10.12989/aas.2018.5.6.615.

EC